



Adsorption of 2,4,6-trichlorophenol by magnetic mesoporous SiO₂ and the adsorption capacity regeneration by UV photolysis

Jie Cui^{a,b}, Xiaoliang Ma^b, Xiaogang Wu^{a,*}, Xu Zhang^{b,*}

^aSchool of Urban Construction, Yangtze University, Jingzhou 434023, P.R. China, Tel. +86 2768772910; Fax: +86 2768778893; email: wxgglobes@163.com (X. Wu)

^bSchool of Resources and Environmental Science, Wuhan University, Wuhan 430079, P.R. China, email: xuzhangwhu@gmail.com (X. Zhang)

Received 2 October 2014; Accepted 8 January 2015

ABSTRACT

The adsorption of 2,4,6-trichlorophenol (2,4,6-TCP) on synthesized magnetic mesoporous silica (Fe₃O₄/SiO₂/m-SiO₂, MMS) composites and the regeneration of its adsorption capacity through direct UV photolysis was performed in this work. MMS exhibited good performance in removing 2,4,6-TCP from aqueous solutions. The adsorption ratio of 2,4,6-TCP was determined to be influenced by aquatic pH, dissolved humic acids, ionic strength, temperature, and the loaded adsorbents. The adsorption isotherm fit the Freundlich and Polanyi–Manes model better than the Langmuir model, which indicated that the adsorption of 2,4,6-TCP was more likely a pore-filling process. The calculated adsorbed capacity for 2,4,6-TCP on MMS was 55 mg/g. Direct UV photolysis could decompose the adsorbed 2,4,6-TCP and later regenerate the adsorption capacity of MMS to a certain degree; however, the outer mesoporous silica layer was not UV-persistent, and large parts of the mesoporous silica layer were also shown to be corrupted from the Fe₃O₄/SiO₂ core. Therefore, after long duration UV irradiation, the adsorption of 2,4,6-TCP on regenerated MMS was much lower than on freshly synthesized MMS. These results suggest that the photostability of magnetic core-shell-like nanocomposites should be investigated because parts of the composites might leach into the bulk phase during practical use and cause potential environmental risks, similar to other well-known nanomaterials.

Keywords: 2,4,6-trichlorophenol; Adsorption; Magnetic mesoporous silica; UV regeneration

1. Introduction

Chlorophenols are considered as a type of highly toxic, carcinogenic, and persistent pollutant and are widely used in pesticides, antiseptics, and wood preservers [1]. Among all chlorophenols, 2-chlorophenol (2-CP), 2,4-dichlorophenol (2,4-DCP), and 2,4,6-trichlorophenol (2,4,6-TCP) are the most frequently detected

in drinking water due to their production as by-products of disinfection [1]. Chlorophenols can enter the environment during their manufacturing, transport, or use and cause undesired effects on organisms even at trace levels [2]. Chlorophenols have thus been characterized as important pollutants by many governments. Both biological and chemical remediation methods have been investigated to remove chlorophenols from aquatic solutions [3–6]. Hydroxyl-radical-based (·OH)

*Corresponding authors.

advanced oxidation technology is the most powerful method to decompose various phenolic compounds. However, results from this technology demonstrate that chlorophenols are more persistent than other substituted phenols, including methylphenols, nitrophenols, and aminophenols [7]. The substitution position and number of chlorine atoms also showed great influence on the degradation of chlorophenols [6,8].

Conversely, research has shown that adsorption could be an alternative method for the fast removal of chlorophenols, particularly when large volumes of chlorophenols in aqueous solutions need to be removed. Active carbons were the most commonly used adsorbents; the adsorption capacities for 2,4,6-TCP were between 100 and 700 mg/g [9–11]. The adsorption of chlorophenols by other sorbents including carbon nanotubes [12], graphene oxide [13], modified clay minerals [14], and zeolites [15,16] were also investigated; their adsorption capacities were found to be between 10 and 200 mg/g. All these adsorbents require centrifugation to achieve aqueous adsorbents separation in the slurry operation method, making them inconvenient to treat large volumes of wastewater.

In recent decades, various magnetic mesoporous nanocomposites (MMNPs) with well-defined mesoporous structures, shapes, and tailored properties were synthesized and characterized because of their potential application in healthcare, drug delivery, industry, and environmental remediation [17,18]. MMNPs have also been used as adsorbents due to their high specific surface area and easy recyclability. The adsorption capacity of methyl orange onto mesoporous magnetic Co/carbon nanocomposites could reach 380 mg/g [19]. MMNPs also possess good adsorption capacity for the removal of inorganic pollutants [20,21]. However, compared with the wide investigation of the adsorption of chlorophenols compared to other adsorbents, the study on the adsorption of chlorophenols over MMNPs was limited [22,23].

The synthesis of MMNPs requires more time and typically has a higher cost than that of other nanoparticles. Therefore, regeneration and reuse of MMNPs are an important issue that should be researched. Electrothermal desorption, liquid elution, microwave sonication, and chemical oxidation have been applied to regenerate adsorbents [16,24,25]. Zhang et al. showed that ozone oxidation can be a successful method of regenerating the adsorption capacity of FAU-type zeolite for the removal of 2,4,6-TCP; the specific surface area could also be enhanced after ozone oxidation [16]. However, ozone oxidation was shown to not be suitable for the regeneration of all adsorbents. Valdés et al. found that the adsorption of methylene blue on

active carbon decreased after ozone treatment because of changes in its structural properties [26]. This is thus worthwhile to investigate the ability of other methods such as UV photolysis, to regenerate the adsorption capacity of adsorbents.

In this work, magnetic mesoporous silica (MMS, $\text{Fe}_3\text{O}_4/\text{SiO}_2/\text{m-SiO}_2$) was synthesized and its structure was systematically characterized. The adsorption kinetics and capacity of 2,4,6-TCP over MMS and the parameters that influence adsorption were investigated. Conversely, the performance of direct UV photolysis in regenerating the adsorption capacity of MMS and its structural changes after regeneration was also investigated in this work.

2. Materials and methods

2.1. Reagents

2,4,6-trichlorophenol (98%) was obtained from the Aladdin reagent Corporation (Shanghai, China) and used as a representative of chlorophenol pollutants. $\text{FeCl}_3 \cdot 6\text{H}_2\text{O}$, sodium acetate ($\text{NaAc} \cdot 3\text{H}_2\text{O}$), tetraethyl orthosilicate (TEOS), ethylene glycol, absolute ethanol, concentrated aqueous ammonia solution, and hydrochloric acid were purchased from Sinopharm Chemical Reagent Co. Ltd (Shanghai, China). All reagents were analytical grade and used without further purification. Commercial humic acid (Sigma-Aldrich, sodium salt) was purified before use according to the previous work [27]. Deionized water with a resistivity of greater than $18.0 \text{ M}\Omega \text{ cm}$ was used during sample preparation.

2.2. Synthesis of $\text{Fe}_3\text{O}_4/\text{SiO}_2/\text{m-SiO}_2$

Fe_3O_4 core and $\text{Fe}_3\text{O}_4/\text{SiO}_2$ were synthesized according to reported methods; the details of this procedure have been described in the authors' previous work [28]. $\text{Fe}_3\text{O}_4/\text{SiO}_2/\text{m-SiO}_2$ was synthesized according to the methods reported by Xu et al. with little modification [29]. About 0.1 g $\text{Fe}_3\text{O}_4/\text{SiO}_2$ was added to 80 mL deionized water, 60 mL ethanol, 1.0 g concentrated ammonia aqueous solution, and 0.3 g hexadecyltrimethylammonium bromide (CTAB). The suspension was homogenized for 0.5 h to form a uniform dispersion with sonication; the resulting solution was then transferred to a 250 mL three-necked round-bottom flask. After mechanical stirring for 10 min at 1,000 rpm, 0.4 g TEOS was added dropwise to the above solution. The reaction was allowed to proceed at room temperature for 6 h. The solids were then separated from the dispersion by a magnet and washed repeatedly with ethanol, water, and acetone to remove

nonmagnetic by-products. Then, the magnetic nanocomposites were redispersed in 60 mL of acetone and refluxed at 80°C for 48 h to remove the template CTAB; this extraction procedure was repeated three times. The obtained Fe₃O₄/SiO₂/m-SiO₂ was then washed with deionized water three times and then dried in a vacuum at 60°C for 6 h.

2.3. Characterization of synthesized magnetic materials

The Brunauer–Emmett–Teller (BET) surface area was determined by a Micromeritics ASAP 2020 setup. The XRD patterns of the prepared products were recorded with a Dmax-rA powder diffractometer (Rigaku, Japan), which used a Cu K α radiation source at a scanning rate of 2° min⁻¹. Scanning electron micrographs (SEM) and energy-dispersive X-ray spectroscopy (EDS) were taken with a FEI-QUANTA 200 microscope. Transmission electron microscopy (TEM) images were obtained on a JEOL JEM 2010HT microscope (Japan Electronics, Japan) at an accelerating voltage of 200 kV. The zeta potential of MMS in the presence and in the absence of 2,4,6-TCP was determined using a Zetasizer 3600 (Malvern Instrument).

2.4. Adsorption of 2,4,6-trichlorophenol on Fe₃O₄/SiO₂/m-SiO₂

2.4.1. Adsorption kinetics

0.5 g/L MMS was directly added to a 50 mL 2,4,6-TCP solution (50 μ M), and the dispersion was shaken at room temperature. Two milliliter samples were withdrawn from the flask at different time intervals. The MMS and aqueous solution was quickly separated by a magnet, and the concentration of 2,4,6-TCP in the supernatant was analyzed by HPLC. The effects of pH, MMS dosage, and humic acids on the adsorption of 2,4,6-TCP were performed in the same way. The pH value of the suspended solution was adjusted by the addition of dilute HCl or NaOH solutions (0.1 M).

2.4.2. Adsorption isotherm

Batch adsorption studies were performed using aqueous suspensions containing 2,4,6-TCP with different initial concentrations (i.e. with C_0 from 40 to 100 μ M) and 0.5 g/L of MMS. The suspension was continuously stirred using a constant temperature mechanical stirrer for 12 h. After reaching equilibrium, 2 mL aliquots of the suspensions were withdrawn to determine the equilibrium concentration C_t . The adsorption isotherm experiments were carried out at pH 6.0 without adding any electrolytes.

2.5. Regeneration of adsorption capacity of MMS by UV photolysis

The dispersion was poured to a petridish after reaching the adsorption equilibrium, and MMS with adsorbed 2,4,6-TCP was separated from the aqueous solution by a magnet place at the bottom of the dish. The supernatant was discarded and the solids were then irradiated under direct UV (254 nm) irradiation for 30 min by using a Philips TUV PLS 9 W lamp as the irradiation source. The MMS particles were mixed several times by moving the magnet. After irradiation, the MMS particles were washed by pure water and then directly redispersed in a 50 μ M 2,4,6-TCP solution to investigate its cycling performance. Control experiments showed the adsorbed 2,4,6-TCP could be fully extracted by using ethanol. On the other side, no 2,4,6-TCP could be extracted by ethanol from the irradiated MMS, thus indicating adsorbed 2,4,6-TCP was decomposed after 30 min irradiation.

2.6. Sample analysis and data analysis

2.6.1. Sample analysis

The concentrations of 2,4,6-TCP were determined using the reversed-phase HPLC method. Experiments were performed using a Waters 484 HPLC with an Agilent Zorbax SB-C18 column (5 μ m, 4.6 \times 150 mm). The mobile phase was a mixed solution of methanol water and acetic acid (v/v/v = 80/19/1) with a flow rate of 1.0 mL/min. The UV detection wavelength was set at 280 nm. The retention time for 2,4,6-TCP was 4.5 min, and its concentration was determined by the working curve method from 0.1 to 150 μ mol/L.

2.6.2. Data analysis

The adsorbed 2,4,6-TCP per gram of MMS at different times (q_t , μ mol/g) and at the equilibrium time (q_e , μ mol/g) were, respectively, calculated from Eqs. (1) and (2):

$$q_t = \frac{(c_0 - c_t) \times V}{m} \quad (1)$$

$$q_e = \frac{(c_0 - c_e) \times V}{m} \quad (2)$$

where c_0 , c_t , and c_e are the initial concentration, concentration at different times, and the equilibrium concentration of 2,4,6-TCP (μ mol/L), respectively.

The adsorption ratio (%) of 2,4,6-trichlorophenol was calculated from Eq. (3):

$$R = \left(1 - \frac{c_e}{c_0}\right) \times 100\% \quad (3)$$

The Freundlich (Eq. (4)), Langmuir (Eq. (5)), and Polanyi-Manes model (PMM) (Eq. (6)) isotherms were used to describe the adsorption properties of 2,4,6-trichlorophenol on MMS as [30]:

$$q_e = K_F \times c_e^{1/n} \quad (4)$$

where K_F ($(\mu\text{mol/g}) (\text{L/g})^{1/n}$) is the Freundlich affinity coefficient and $1/n$ represents the Freundlich exponential coefficient. It also can be said that:

$$q_e = \frac{q_{\max} \times K_L \times c_e}{1 + K_L \times c_e} \quad (5)$$

where q_{\max} ($\mu\text{mol/g}$) is the maximum adsorption of 2,4,6-trichlorophenol on MMS and K_L ($\text{L}/\mu\text{mol}$) is the Langmuir adsorption constant. It can be written that:

$$\log q_e = \log Q^0 + a(\varepsilon_{\text{SW}}/V_s)^b \quad (6)$$

$$\varepsilon_{\text{SW}} = RT \ln (c_s/c_e) \quad (7)$$

where ε_{SW} (kJ/mol) is the adsorption potential, which can be calculated from Eq. (7); c_s ($\mu\text{mol/L}$ or mg/L) is

the aqueous water solubility; V_s (cm^3/mol) is the molar volume of the solute; Q^0 is the adsorption capacity; a and b are fitting parameters; R is the universal gas constant; and T is the absolute temperature.

All experiments were performed three times and described as a mean \pm standard deviation. The regression of the experimental data was calculated using Origin 8.5 software.

3. Results and discussion

3.1. Morphology of MMS

The morphology of the magnetic cores and corresponding MMSs was firstly investigated by SEM and TEM. As shown in Fig. 1(a), the diameter of the magnetic core Fe_3O_4 is approximately 380 nm. The first coated layer is a nonporous silica layer that protects the magnetic core from acid corruption; the typical thickness of this silica layer is approximately 5 nm (Fig. 1(b)). A CTAB/ SiO_2 layer was then successfully coated onto the $\text{Fe}_3\text{O}_4/\text{SiO}_2$ microsphere surface through surfactant-templating process (Fig. S1, Supporting Information). The absorbance peaks at 2,923.0 and 2,826.7 cm^{-1} that belong to the vibrations of $-\text{CH}_2$ of CTAB templates vanished after acetone extraction; this is also shown in the EDS elemental maps (Fig. S2, Supporting Information), indicating that the CTAB templates were successfully removed. XRD patterns (Fig. S3, Supporting Information) indicating the

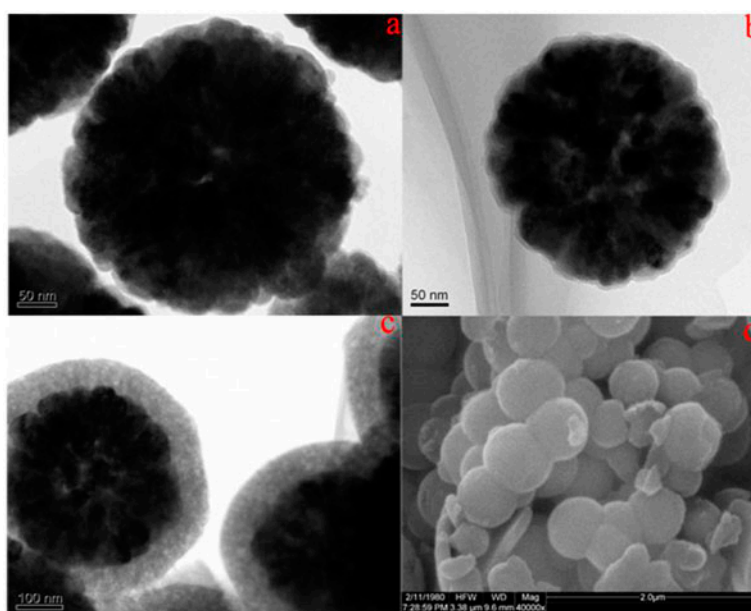


Fig. 1. TEM images of (a) Fe_3O_4 particles; (b) $\text{Fe}_3\text{O}_4/\text{SiO}_2$; (c) $\text{Fe}_3\text{O}_4/\text{SiO}_2/\text{m-SiO}_2$ composites; and (d) SEM image of $\text{Fe}_3\text{O}_4/\text{SiO}_2/\text{m-SiO}_2$ composites.

magnetic core exhibited hardly any phase change after coating with either a nonporous silica layer or the mesoporous silica shell. The thickness of the uniform mesoporous silica shell in the outer sphere is approximately 60 nm (Fig. 1(c)), which was near the reported thickness of approximately 70 nm [31]. The SEM images demonstrate that the MMS particles are uniform in both size and shape (Fig. 1(d)).

3.2. BET analysis of MMS

The N_2 adsorption/desorption isotherms of MMS shown in Fig. 2 exhibit type IV isotherms with a H_1 -type hysteresis loop, which are characteristic of mesopores with very uniform pore size [32,33]. The BET surface area for MMS is $75.6 \text{ m}^2/\text{g}$, which is much larger than Fe_3O_4 core ($9.5 \text{ m}^2/\text{g}$) and $\text{Fe}_3\text{O}_4/\text{SiO}_2$ ($14.6 \text{ m}^2/\text{g}$). The Barrett–Joyner–Halenda (BJH) pore size distribution curves calculated from the desorption branches are presented in the inset figure. It is clearly shown that the mesopore size of MMS exhibits a narrow distribution centered at approximately 3.5 nm. The BJH total pore volume of MMS is $0.11 \text{ cm}^3/\text{g}$.

3.3. Adsorption equilibrium of 2,4,6-trichlorophenol on MMS

Equilibrium adsorption studies were investigated, and the resulting influences of contact time on the adsorption of 2,4,6-TCP onto MMS have been determined and are illustrated in Fig. 3. The adsorbed 2,4,6-TCP is shown to increase and the corresponding bulk concentration of 2,4,6-TCP quickly decreases with time up to 10 min, reaching equilibrium within 30 min for MMS. The adsorption kinetics were then fit with

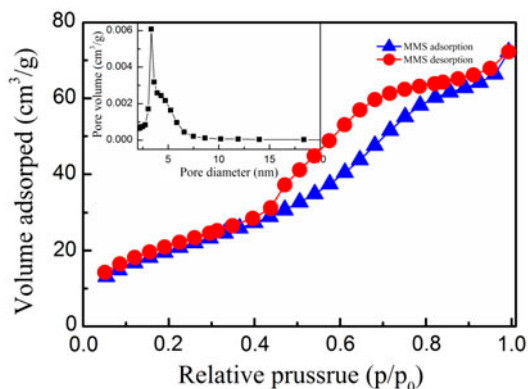


Fig. 2. N_2 adsorption–desorption isotherms of $\text{Fe}_3\text{O}_4/\text{SiO}_2/\text{m-SiO}_2$ composite; inset shows the mesopore size distribution.

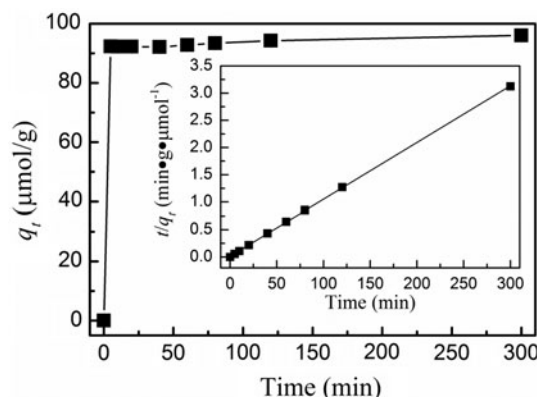


Fig. 3. Dependence of adsorbed 2,4,6-TCP per gram MMS (q_e) on contact time (in 0.5 g/L MMS dispersions); inset shows the adsorption kinetics of 2,4,6-TCP on MMS; the lines correspond to the data fit to the pseudo-second-order kinetic mode.

different equations including pseudo-first-order and pseudo-second-order models. The correlation coefficient (r^2) for the pseudo-second-order kinetic model is higher than 0.999, which suggests that the pseudo-second-order model is an adequate method to describe the adsorption process of 2,4,6-TCP to MMS (see inset of Fig. 1). The calculated adsorption kinetic constant is $0.01 \text{ g}/\mu\text{mol min}$, and the approaching equilibrium factor (R_w) is 0.032 [34]. The R_w indicates that the adsorption process of 2,4,6-TCP to MMS is approaching equilibrium.

3.4. Effects of loaded MMS and humic acids on the adsorption of 2,4,6-trichlorophenol

The effects of loaded MMS and humic acid concentrations on the adsorption of 2,4,6-TCP to MMS are shown in Fig. 4. The adsorption ratios of 2,4,6-TCP increase quickly with an increase in loaded MMS from 0 to 0.5 g/L. The adsorption rate increases to approximately 100% with a further increase in MMS up to 1.0 g/L. The increase of adsorption rate with the increase of loaded MMS is likely caused by additional adsorption sites being available for 2,4,6-TCP.

Conversely, the adsorption ratios of 2,4,6-TCP decrease with an increase in humic acid concentrations, which is representative of dissolved organic matter in aquatic solutions. The adsorption ratios were 94 and 78% in the absence and the presence of 50 mg/L HA, respectively. The effects of HA on the adsorption of 2,4,6-TCP to MMS are thus shown to be consistent with its effects on the adsorption of 2,4,6-TCP to magnetic mesoporous carbon. The adsorption capacity of magnetic mesoporous carbon for 2,4,6-TCP

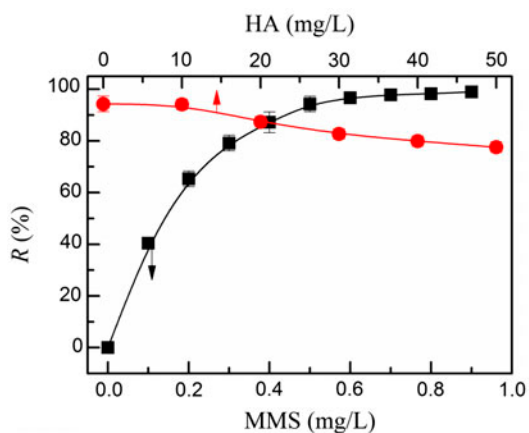


Fig. 4. Effects of loaded MMS and dissolved humic acid on the adsorption of 2,4,6-TCP on MMS, pH = 6.0.

decreases by one third with the addition of 50 mg/L HA [22]. The various functional groups in humic acids, including carboxylic and hydroxyl groups, are expected to interact strongly with the surface of metal oxides through different interactions. Bulk and adsorbed HA exhibit different influences on the adsorption of organic pollutants to that of nanoparticles; their influences could also be changed due to the interaction between organic pollutants and HA. Bulk HA could compete for adsorption sites with organic pollutants, causing a decrease in the adsorption of organic pollutants [35]. Conversely, the adsorbed HA could enhance the adsorption of organic pollutants if the interaction between HA and organic pollutants was strong, and organic pollutants have a low adsorption affinity on the adsorbents [36]. In this work, dissolved HA could compete for the adsorption sites with 2,4,6-TCP and thereafter inhibit the adsorption of 2,4,6-TCP on MMS.

3.5. Effects of aquatic pH on the adsorption of 2,4,6-trichlorophenol

The effects of aquatic pH could change the distribution of adsorbates and the surface charge of adsorbents following the influence on adsorption. As shown in Fig. 5, aquatic pH showed a great influence on the adsorption of 2,4,6-TCP on MMS and the distribution of 2,4,6-TCP in aqueous solution. 2,4,6-TCP mainly exists in a neutral form below a pH of 6.23, but exists in the phenolic anion form at pHs higher than 6.23. The adsorption was much larger near neutral pH than in acidic or basic solutions. The adsorption ratios of 2,4,6-TCP on MMS were 72, 94, and 40% in a pH solution at 4.0, 6.0, and 10.0, respectively. The adsorption of 2,4,6-TCP on other adsorbents including active

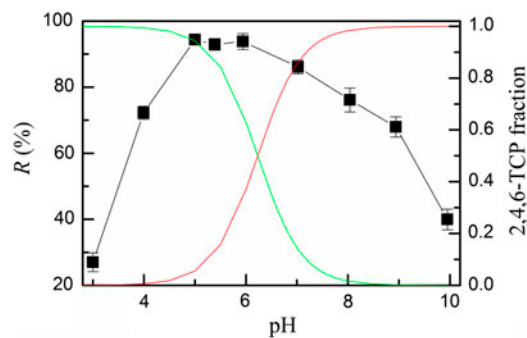


Fig. 5. Dependence of 2,4,6-TCP adsorption rate (R , %) over MMS and norfloxacin exist form with solution pH.

carbon, multi-walled carbon nanotubes, graphene oxide, zeolite, and soils was found to be lower in basic solutions [9–11,16,22,37,38].

Zeta potential values were measured in aqueous solutions to further investigate the mechanism of adsorption of 2,4,6-TCP to MMS. The values of zeta potential as a function of pH are shown in Fig. 6. The points of zero charges (PZC) for MMS before and after adsorption are 4.7 and 5.3, respectively. The adsorption of 2,4,6-TCP on MMS shifts the PZC to a more positive position, which suggests a strong interaction between 2,4,6-TCP and MMS near PZC. The surface of MMS was positively charged when the pH was lower than the PZC and 2,4,6-TCP existed in neutral form; the relatively lower adsorption rate in acidic solution might be caused by competitive adsorption between protons and 2,4,6-TCP. Conversely, the surface of MMS was negatively charged, and 2,4,6-TCP existed in its phenolic anion form when the solution pH was higher than 6.23. Thus, the electrostatic repulsion generated between the anion and the surface charge

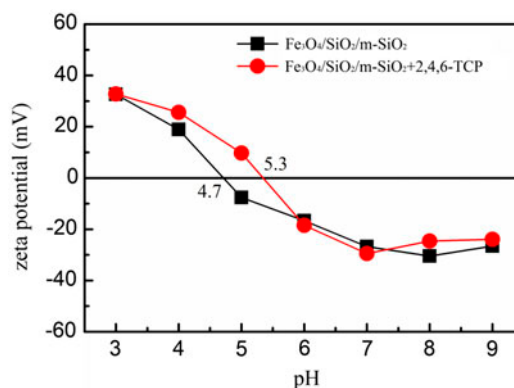


Fig. 6. Zeta potential of suspended MMS particle in aqueous solution as a function of pH in the absence and in the presence of 50 μ M 2,4,6-TCP.

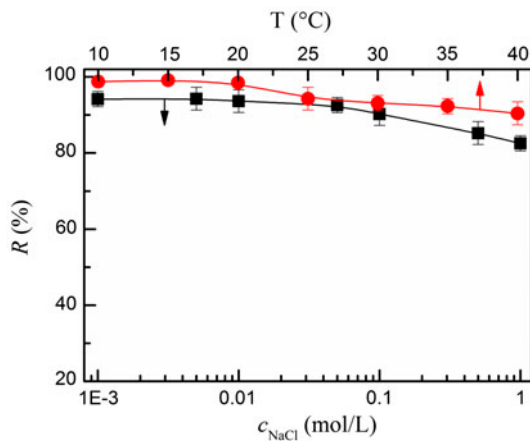


Fig. 7. Effects of ionic strength and temperature on the adsorption of 2,4,6-TCP to MMS, pH = 6.0.

contributes to a low adsorption rate in basic solutions. Conversely, surface of MMS and 2,4,6-TCP was not charged in the solution near a pH of 5.0, and thereafter, the adsorption ratios were relatively higher.

3.6. Effects of ionic strength and temperature on the adsorption of 2,4,6-trichlorophenol

The effects of ionic strength on the adsorption of 2,4,6-TCP to MMS were carried out by adding different NaCl (from 0.001 to 1 mol/L) into the solution. As shown in Fig. 7, there is no significant difference in the adsorption ratios with the increase of NaCl concentration to 0.05 mol/L. A slight decrease in adsorption ratio occurred with further increase of NaCl concentration to 0.1 mol/L. The adsorption ratio was 82.5% in the presence of 1 mol/L NaCl. The results indicated that the interaction between 2,4,6-TCP and MMS was stronger than nonspecific electrostatic interactions. The adsorption ratios were all higher than 90.0% for the experiments carried out from 10 to 40°C, indicating the effect of temperature on the adsorption of 2,4,6-trichlorophenol was insignificant.

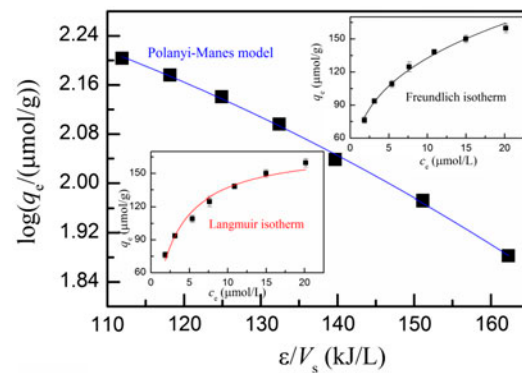


Fig. 8. Dependence of the adsorbed 2,4,6-TCP per gram MMS (q_e) with the equilibrium concentration (c_e). The solid lines correspond to the fits of the data to Polanyi-Manes model. Inset showed the fits of the data to Langmuir and Freundlich isotherm models.

3.7. Adsorption isotherm of 2,4,6-trichlorophenol on MMS

The Freundlich, Langmuir, and PMM techniques are usually used to describe the adsorption properties of pollutants with various adsorbents. The isotherms of TCP on MMS predicted from all three models are fit in Fig. 8. The fitting results for the adsorption of 2,4,6-TCP on MMS are listed in Table 1.

The Langmuir isotherm is mainly applied to model a monolayer adsorption on adsorbents with homogeneous and energetically uniform surfaces. In this work, the Langmuir model showed significant deviation from the experimental data at high concentrations (Fig. 8). As listed in Table 1, the fitting of the experimental data using the Langmuir model yields the lowest correlation coefficients (R^2), which indicates that the Langmuir isotherm model was not suitable to describe the adsorption equilibrium of 2,4,6-TCP on MMS. Thus, the adsorption of 2,4,6-TCP on MMS might not only happen on the surface but also within its inner pores. The adsorption of 2,4,6-TCP on magnetic mesoporous carbon was also found to not fit the Langmuir isotherm model well [22].

Table 1

Calculated Langmuir, Freundlich, and PMM isotherm model constants, correlation coefficients (R^2) and Chi-squared values (χ^2) for the adsorption of 2,4,6-TCP on MMS

Isotherm	Fitted parameters		R^2	χ^2
Freundlich	$1/n$ 0.31 ± 0.01	$K_F ((\mu\text{mol/g})/(\mu\text{mol/L})^{1/n})$ 65.5 ± 1.7	0.993	0.763
Langmuir	q_{max} ($\mu\text{mol/g}$) 174 ± 5	K_L (L/ μmol) 0.37 ± 0.04	0.977	2.42
PMM	Q^0 ($\mu\text{mol/g}$) 278 ± 1	$a \times 10^6$ -4.5 ± 8.7	0.998	0.00003
		b 2.3 ± 0.3		

Conversely, the PMM model yields the highest correlation coefficients (R^2) and lowest Chi-squared values (χ^2), which indicates that the PMM isotherm was the most suitable model to describe the adsorption equilibrium of 2,4,6-TCP on MMS. The PMM model was proposed based on Polanyi potential theory and is applicable for both pore-filling and flat surfaces [39]. The adsorption of 2,4,6-TCP on multi-walled carbon nanotubes was also best fit by the PMM [12]. The results also showed that the isotherm data fit the Freundlich model well ($R^2 = 0.993$). The value of $1/n$ is less than 1, which indicates that the adsorption of 2,4,6-TCP on MMS was a favorable sorption.

3.8. Performance of UV photolysis on the regeneration of adsorption capacity of MMS

The adsorption capacity of MMS was regenerated by UV irradiation in this work. After reached adsorption equilibrium, MMS particles were recovered by magnet, and irradiated under UV irradiation for 30 min. MMS was washed with deionized water, magnetic separated, dried, and weighted after irradiation and then redispersed in freshly prepared 2,4,6-TCP. As shown in Fig. 9, during the MMS's second use, the

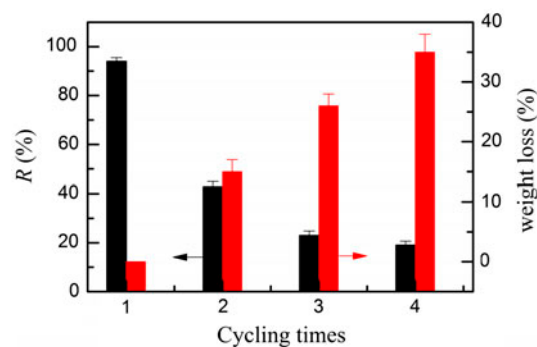


Fig. 9. Dependence of 2,4,6-TCP adsorption rate (R , %) and the mass loss of MMS with the adsorption/regeneration times.

adsorption ratio of 2,4,6-TCP on MMS was 43%, which was approximately half of the adsorption of freshly made MMS. The adsorption ratio further decreased to approximately 20% in the third and fourth uses of the MMS. Conversely, it was also found that magnetic mass is also lost with an increase in irradiation time. After three adsorption/regeneration uses, the MMS lost approximately 30% of its weight.

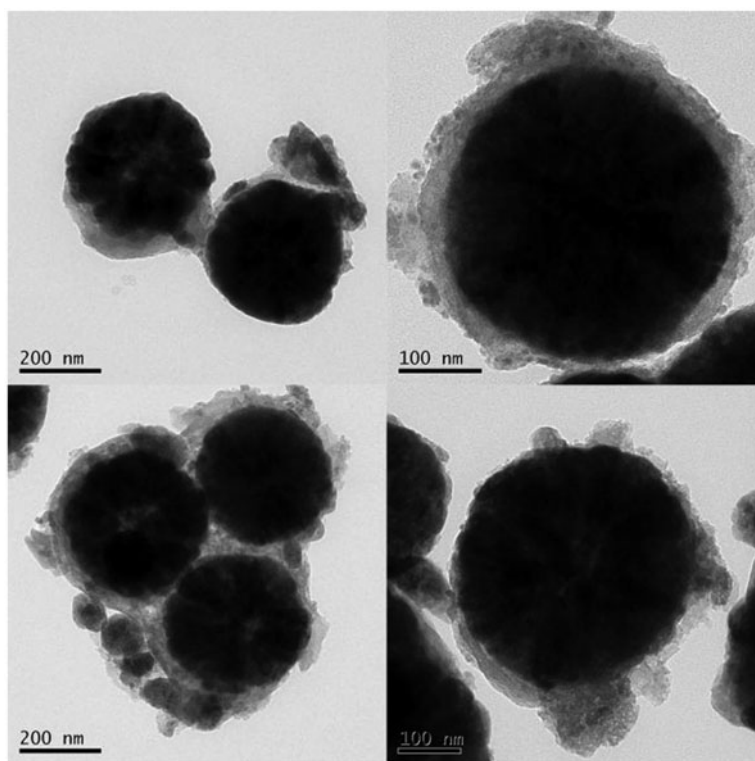


Fig. 10. TEM images of $\text{Fe}_3\text{O}_4/\text{SiO}_2/\text{m-SiO}_2$ microsphere after 5 h UV irradiation.

These results indicate that the MMS was not stable under UV irradiation. Therefore, the morphology of the used MMS was reanalyzed by TEM. As shown in Fig. 10, the magnetic core did not change significantly after four cycles. However, the outer sphere, which is made of mesoporous silica, was corrupted to different extents compared to the freshly made MMS. Thus, parts of the mesoporous silica leached into the bulk phase during the washing process after UV irradiation, thus reducing the adsorption ratio of 2,4,6-TCP. On the other side, it should be noted that the accumulated intermediates generated during the UV photolysis of adsorbed 2,4,6-TCP may also contribute to the decline of MMS's adsorption capacity.

4. Conclusion

The synthesized magnetic mesoporous silica (MMS, $\text{Fe}_3\text{O}_4/\text{SiO}_2/\text{m-SiO}_2$) was uniform in both size and shape, as shown by SEM and TEM. The diameter of the magnetic core Fe_3O_4 is approximately 380 nm, and the thickness of the coated nonporous silica layer and mesoporous silica shell is approximately 5 and 60 nm, respectively. MMS showed good adsorption capacity to 2,4,6-TCP. The adsorption of 2,4,6-TCP on MMS followed the pseudo-second-order model and adsorption was shown to be pH dependent. The adsorption of 2,4,6-TCP in the solution with a pH near the PZC for MMS (~5.0) was larger than that in acidic or basic solutions. The presence of up to 50 mg/L dissolved humic acid was shown to slightly inhibit adsorption. The adsorption of 2,4,6-TCP on MMS fits the Freundlich and PMM well but fits the Langmuir model poorly. The adsorption capacity of MMS was only partly regenerated by UV direct photolysis because the magnetic composites were not stable under UV irradiation, and the mesoporous silica shell was corrupted. The regeneration of the adsorption capacity of MMS by other chemical oxidation methods is currently being investigated by the authors.

Acknowledgments

This work has been supported by the National Natural Science Foundation of China (Grant No. 21207104) and the Hubei Provincial Department of Education Science Technology Research Project (Grant No. Q20141309).

Supplemental data

Supplemental data for this article can be accessed here <http://dx.doi.org/10.1080/19443994.2015.1009173>.

References

- [1] WHO, Chlorophenols in drinking-water. Background Document for Preparation of WHO Guidelines for Drinking-water Quality, World Health Organization, Geneva, 2003.
- [2] W.E. Peplko, D.W. Gaylor, D. Mukerjee, Comparative toxic potency ranking of chlorophenols, *Toxicol. Ind. Health*. 21 (2005) 93–111.
- [3] A. Musa, M. Ba-Abbad, A. Kadhum, A. Mohamad, Photodegradation of chlorophenolic compounds using zinc oxide as photocatalyst: Experimental and theoretical studies, *Res. Chem. Intermed.* 38 (2012) 995–1005.
- [4] C. Chin Wang, C. Mei Lee, C. Jen Lu, M. Shang Chuang, C. Zong Huang, Biodegradation of 2,4,6-trichlorophenol in the presence of primary substrate by immobilized pure culture bacteria, *Chemosphere* 41 (2000) 1873–1879.
- [5] Z. Xiong, Y. Xu, L. Zhu, J. Zhao, Enhanced photodegradation of 2,4,6-trichlorophenol over palladium phtalocyaninesulfonate modified organobentonite, *Langmuir* 21 (2005) 10602–10607.
- [6] L.P. Huang, Y.H. Shi, N. Wang, Y.S. Dong, Anaerobic/aerobic conditions and biostimulation for enhanced chlorophenols degradation in biocathode microbial fuel cells, *Biodegradation* 25 (2014) 615–632.
- [7] C. Karunakaran, R. Dhanalakshmi, Substituent effect on nano TiO_2 - and ZnO -catalyzed phenol photodegradation rates, *Int. J. Chem. Kinet.* 41 (2009) 275–283.
- [8] S. Antonaraki, E. Androulaki, D. Dimotikali, A. Hiskia, E. Papaconstantinou, Photolytic degradation of all chlorophenols with polyoxometallates and H_2O_2 , *J. Photochem. Photobiol., A* 148 (2002) 191–197.
- [9] B.H. Hameed, I.A.W. Tan, A.L. Ahmad, Adsorption isotherm, kinetic modeling and mechanism of 2,4,6-trichlorophenol on coconut husk-based activated carbon, *Chem. Eng. J.* 144 (2008) 235–244.
- [10] I.A.W. Tan, A.L. Ahmad, B.H. Hameed, Adsorption isotherms, kinetics, thermodynamics and desorption studies of 2,4,6-trichlorophenol on oil palm empty fruit bunch-based activated carbon, *J. Hazard. Mater.* 164 (2009) 473–482.
- [11] J. Fan, J. Zhang, C. Zhang, L. Ren, Q. Shi, Adsorption of 2,4,6-trichlorophenol from aqueous solution onto activated carbon derived from loosestrife, *Desalination* 267 (2011) 139–146.
- [12] G.-C. Chen, X.-Q. Shan, Y.-S. Wang, B. Wen, Z.-G. Pei, Y.-N. Xie, T. Liu, J.J. Pignatello, Adsorption of 2,4,6-trichlorophenol by multi-walled carbon nanotubes as affected by Cu(II), *Water Res.* 43 (2009) 2409–2418.
- [13] V. Chandra, J. Park, Y. Chun, J.W. Lee, I.-C. Hwang, K.S. Kim, Water-dispersible magnetite-reduced graphene oxide composites for arsenic removal, *ACS Nano* 4 (2010) 3979–3986.
- [14] H. Zaghouane-Boudiaf, M. Boutahala, S. Sahnoun, C. Tiar, F. Gomri, Adsorption characteristics, isotherm, kinetics, and diffusion of modified natural bentonite for removing the 2,4,5-trichlorophenol, *Appl. Clay Sci.* 90 (2014) 81–87.
- [15] M. Motsa, J. Thwala, T.M. Msagati, B. Mamba, Adsorption of 2,4,6-trichlorophenol and ortho-nitrophenol from aqueous media Using surfactant-modified clinoptilolite–polypropylene hollow fibre composites, *Water Air Soil Pollut.* 223 (2012) 1555–1569.

- [16] Y. Zhang, R.G. Mancke, M. Sabelfeld, S.-U. Geißen, Adsorption of trichlorophenol on zeolite and adsorbent regeneration with ozone, *J. Hazard. Mater.* 271 (2014) 178–184.
- [17] V. Mamaeva, C. Sahlgren, M. Lindén, Mesoporous silica nanoparticles in medicine—Recent advances, *Adv. Drug Delivery Rev.* 65 (2013) 689–702.
- [18] J. Liu, S.Z. Qiao, Q.H. Hu, G.Q. Lu, Magnetic nanocomposites with mesoporous structures: Synthesis and applications, *Small* 7 (2011) 425–443.
- [19] P. Zhang, Q. An, J. Guo, C.-C. Wang, Synthesis of mesoporous magnetic Co-NPs/carbon nanocomposites and their adsorption property for methyl orange from aqueous solution, *J. Colloid. Interface Sci.* 389 (2013) 10–15.
- [20] M.S. Moorthy, D.-J. Seo, H.-J. Song, S.S. Park, C.-S. Ha, Magnetic mesoporous silica hybrid nanoparticles for highly selective boron adsorption, *J. Mater. Chem. A* 1 (2013) 12485–12496.
- [21] J. Zhu, H. Gu, J. Guo, M. Chen, H. Wei, Z. Luo, H.A. Colorado, N. Yerra, D. Ding, T.C. Ho, N. Haldolaarachchige, J. Hopper, D.P. Young, Z. Guo, S. Wei, Mesoporous magnetic carbon nanocomposite fabrics for highly efficient Cr(vi) removal, *J. Mater. Chem. A* 2 (2014) 2256–2265.
- [22] S. Wang, H. Niu, T. Zeng, X. Ma, Y. Cai, X. Zhao, Fabrication of magnetic mesoporous carbon and its application for adsorptive removal of 2,4,6-trichlorophenol (TCP) from aqueous solution, *Cryst. Eng. Commun.* 16 (2014) 5598–5607.
- [23] P. Yu, Q. Sun, J. Li, J. Pan, Z. Tan, Y. Yan, Synthesis of poly (styrene-divinyl benzene) magnetic porous adsorbents prepared by sulfonation for the adsorption of 2,4-dichlorophenol and 2,4,6-trichlorophenol from aqueous solutions, *Desalin. Water Treat.* (2014) 1–12.
- [24] D. Bathen, Physical waves in adsorption technology—An overview, *Sep. Purif. Technol.* 33 (2003) 163–177.
- [25] R. Cherbański, É. Molga, Intensification of desorption processes by use of microwaves—An overview of possible applications and industrial perspectives, *Chem. Eng. Process.* 48 (2009) 48–58.
- [26] H. Valdés, M. Sánchez-Polo, J. Rivera-Utrilla, C.A. Zaror, Effect of ozone treatment on surface properties of activated carbon, *Langmuir* 18 (2002) 2111–2116.
- [27] Y. Cho, W. Choi, Visible light-induced reactions of humic acids on TiO₂, *J. Photochem. Photobiol. A* 148 (2002) 129–135.
- [28] J. Cui, T. He, X. Zhang, Synthesis of Fe₃O₄@SiO₂@Pt_{ion}-TiO₂ hybrid composites with high efficient UV-visible light photoactivity, *Catal. Commun.* 40 (2013) 66–70.
- [29] X. Xu, C. Deng, M. Gao, W. Yu, P. Yang, X. Zhang, Synthesis of magnetic microspheres with immobilized metal ions for enrichment and direct determination of phosphopeptides by matrix-assisted laser desorption ionization mass spectrometry, *Adv. Mater.* 18 (2006) 3289–3293.
- [30] K. Yang, L. Zhu, B. Xing, Adsorption of polycyclic aromatic hydrocarbons by carbon nanomaterials, *Environ. Sci. Technol.* 40 (2006) 1855–1861.
- [31] Y. Deng, D. Qi, C. Deng, X. Zhang, D. Zhao, Superparamagnetic high-magnetization microspheres with an Fe₃O₄@SiO₂ core and perpendicularly aligned mesoporous SiO₂ shell for removal of microcystins, *J. Am. Chem. Soc.* 130 (2008) 28–29.
- [32] Y. Wang, J. Ren, X. Liu, Y. Wang, Y. Guo, Y. Guo, G. Lu, Facile synthesis of ordered magnetic mesoporous γ -Fe₂O₃/SiO₂ nanocomposites with diverse mesostructures, *J. Colloid Interface Sci.* 326 (2008) 158–165.
- [33] D. He, X. He, K. Wang, Y. Zhao, Z. Zou, Regenerable multifunctional mesoporous silica nanocomposites for simultaneous detection and removal of mercury(II), *Langmuir* 29 (2013) 5896–5904.
- [34] F.C. Wu, R.L. Tseng, S.C. Huang, R.S. Juang, Characteristics of pseudo-second-order kinetic model for liquid-phase adsorption: A mini-review, *Chem. Eng. J.* 151 (2009) 1–9.
- [35] H. Peng, S.X. Feng, X. Zhang, Y. Li, X.Y. Zhang, Adsorption of norfloxacin onto titanium oxide: Effect of drug carrier and dissolved humic acid, *Sci. Total Environ.* 438 (2012) 66–71.
- [36] K. Yang, B. Xing, Sorption of phenanthrene by humic acid-coated nanosized TiO₂ and ZnO, *Environ. Sci. Technol.* 43 (2009) 1845–1851.
- [37] Z.-G. Pei, X.-Q. Shan, T. Liu, Y.-N. Xie, B. Wen, S. Zhang, S.U. Khan, Effect of lead on the sorption of 2,4,6-trichlorophenol on soil and peat, *Environ. Pollut.* 147 (2007) 764–770.
- [38] Z. Pei, L. Li, L. Sun, S. Zhang, X.-Q. Shan, S. Yang, B. Wen, Adsorption characteristics of 1,2,4-trichlorobenzene, 2,4,6-trichlorophenol, 2-naphthol and naphthalene on graphene and graphene oxide, *Carbon* 51 (2013) 156–163.
- [39] K. Yang, X. Wang, L. Zhu, B. Xing, Competitive Sorption of pyrene, phenanthrene, and naphthalene on multiwalled carbon nanotubes, *Environ. Sci. Technol.* 40 (2006) 5804–5810.